

# Hydrophobic Cetyltrimethylammonium Bromide-Pillared Bentonite as an Effective Palm Oil Bleaching Agent

Maria Yuliana,\* Revano J. Sutrisno, Stefanus Hermanto, Suryadi Ismadji, Christian J. Wijaya, Shella P. Santoso, Felycia E. Soetaredjo, and Yi-Hsu Ju



Cite This: *ACS Omega* 2020, 5, 28844–28855



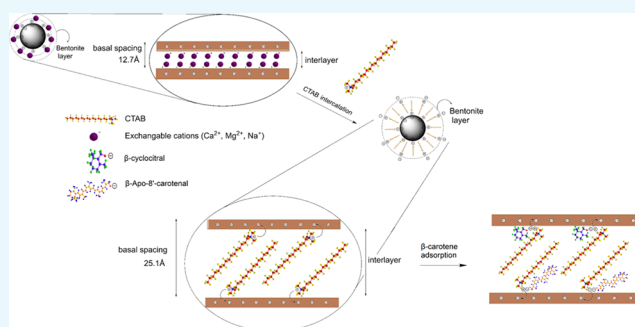
Read Online

ACCESS |

Metrics & More

Article Recommendations

**ABSTRACT:** To promote a minimal use of acid in the activation of bentonite and to maintain oil quality during refinery and storage, a new class of bleaching agent, cetyltrimethylammonium bromide (CTAB)-pillared bentonite (CTAB@Bent), is fabricated. The influences of three independent intercalation variables, including temperature  $T$  (40, 50, and 60 °C), time  $t$  (2, 4, and 6 h), and CTAB loading  $m_c$  (0.2, 0.25, 0.33, 0.50, and 1.00%, w/w), on the  $\beta$ -carotene removal rate are studied. The multilevel factorial design combined with the response surface methodology and three-way analysis of variance is employed to design and optimize experiments in regard to the three independent variables. Based on the optimization results, the highest  $\beta$ -carotene removal rate is monitored at 71.04% (w/w) using CTAB@Bent obtained at optimum intercalation conditions (CTAB@Bent-Opt):  $T = 40$  °C,  $t = 3.2$  h,  $m_c = 1.00\%$  (w/w). The mechanism study shows that the adsorption of  $\beta$ -carotene onto CTAB@Bent-Opt is spontaneous and endothermic, with the governing steps of physical interaction and ion exchange between  $\beta$ -carotene and the cationic head of CTAB. CTAB@Bent-Opt also exhibits characteristics superior to those of commercial raw bentonite and acid-activated bentonite, indicating that a more efficient  $\beta$ -carotene removal can be achieved using this new bleaching agent.



## 1. INTRODUCTION

In 2019, the annual crude palm oil (CPO) production in Indonesia reached 43 million tons, and it was predicted that the production would continually increase in the following 2 years.<sup>1</sup> The enhanced production of CPO is in conjunction with the national demand that continues to grow due to its existence as a source of global vegetable oil and feedstock for the growing biodiesel industry in Indonesia. Palm oil is naturally reddish due to its high  $\beta$ -carotene content (500–700 mg/kg). Removal of this substance is essential to achieve its commercial qualities, namely, light color, bland taste, and excellent oxidative stability.<sup>2–4</sup>

The physical refinery is the most commonly employed technique in palm oil industries and consists of degumming, bleaching, and deodorization steps. The last two steps are equally crucial for  $\beta$ -carotene removal, where bleaching removes a part of the coloring pigments, minor constituents, and oxidation products by adsorption, while deodorization thermally degrades the remaining pigments at high temperature. Among the three major refining steps, bleaching is considered the most critical process and is closely monitored because the significant removal of unwanted materials, including  $\beta$ -carotene,<sup>5</sup> occurs in this step. Moreover, the efficiency of  $\beta$ -carotene removal is regarded as one of the most

important parameters in commercial refineries to determine the overall process efficiency; therefore, the selection of the bleaching agent is deemed crucial.

Raw clays, including bentonite, are vastly developed as multifunctional materials, particularly as an adsorption agent, due to their abundance, low cost, and relatively high purity.<sup>6</sup> Bentonites have found wide applications in adsorption fields because of their superior capacity toward organic and inorganic compounds, particularly the cationic type of substances.<sup>7,8</sup> Various physical characteristics of bentonites, e.g., basal spacing, specific surface area, porous structure, and arrangement models of organic cations, have been reported in numerous studies, with major studies observing the potential correlation between the microstructure of bentonites and their adsorption behavior. Extensive studies have also been conducted to modify the surface and pore structures of the clay materials to increase the adsorption capacity and affinity

Received: August 31, 2020

Accepted: October 19, 2020

Published: October 27, 2020



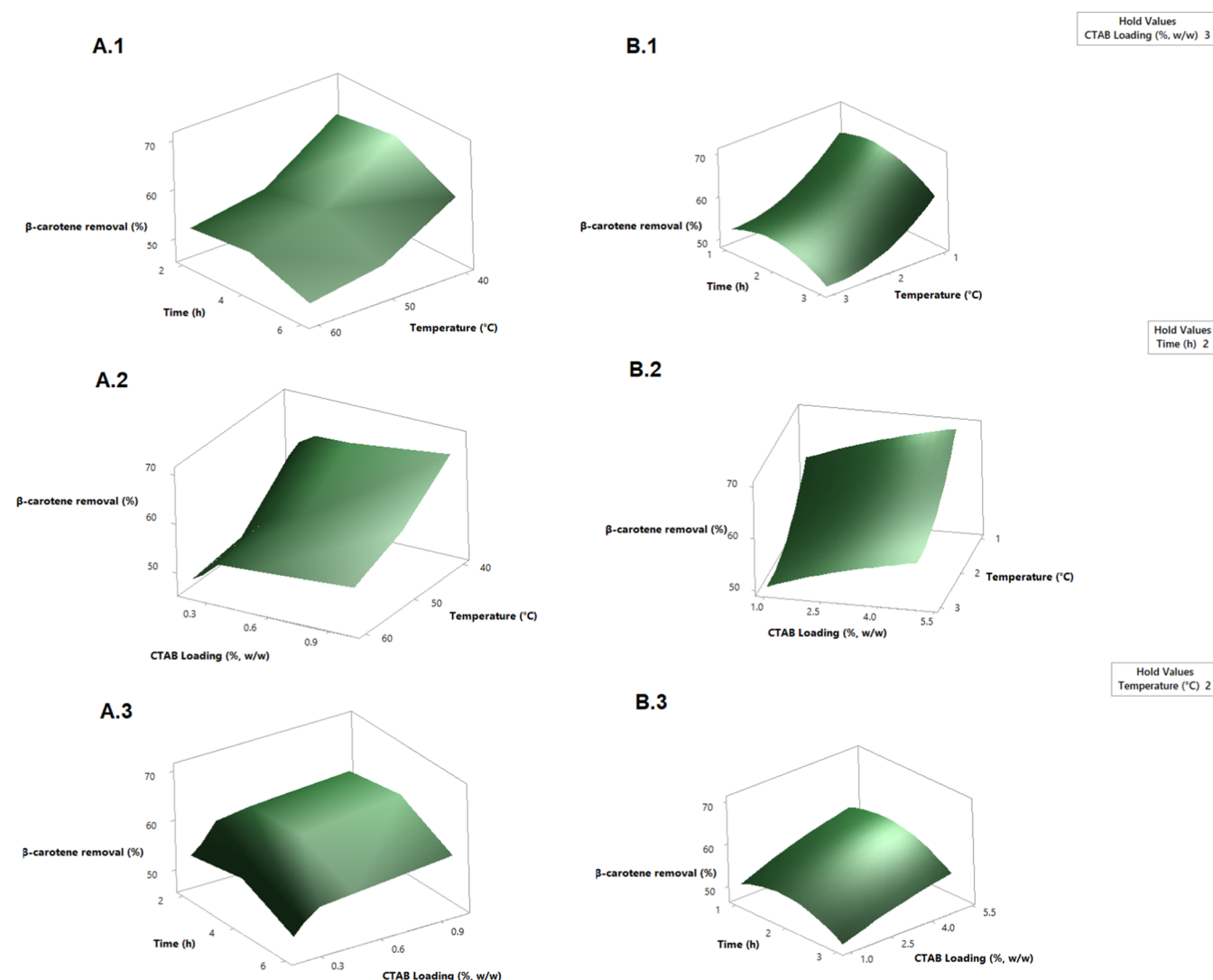


**Figure 1.** Removal rate of  $\beta$ -carotene (% w/w) based on (A) experimental results and (B) 3D response surface plots, with interactions between (1) intercalation temperature  $T$  and time  $t$ , (ii) intercalation temperature  $T$  and CTAB loading  $m_c$ , and (iii) intercalation time  $t$  and CTAB loading  $m_c$ .

toward specific components, with most studies focusing on the acid/base activation method<sup>9,10</sup> due to its straightforwardness. However, the acid/base modification technique induces corrosion of the processing equipment and decrease the oil stability. Excessive use of acid/base during bentonite activation may also cause environmental problems. Therefore, alternative chemical activation is required to create a cleaner and safer technique.

Bentonites are known to possess abundant inorganic cations that are electropositive. This results in the surface being hydrophilic, which tends to attract water to form hydrates.<sup>11</sup> These properties cause natural bentonite to be rarely used in the adsorption of hydrophobic organic compounds. Therefore, surface modification is required to increase the hydrophobicity of bentonites and promote the interaction between bentonites and organic substances. Acikyildiz et al. found that the addition of cetyltrimethylammonium bromide (CTAB) and long-chain hydrocarbons escalates the basal spacing ( $\sim 2$  Å) and hydrophobicity (indicated by the static contact angle of bentonites that reached up to  $150^\circ$ ) of bentonite.<sup>12</sup> Gunawan et al. also reported that an increase in the basal spacing from

12.7 to 24.9 Å was successfully achieved when CTAB was intercalated into the interlayer of bentonite.<sup>13</sup>

While bentonite intercalation has been studied using various surfactants,<sup>14–18</sup> to date, there is no published report on the detailed performance of CTAB-pillared bentonite (CTAB@Bent) for its use in the adsorption of hydrophobic components, specifically  $\beta$ -carotene from CPO. There has also been no report that describes the surface interaction between CTAB@Bent and  $\beta$ -carotene. Bentonite performance as a hydrophobic adsorbent for  $\beta$ -carotene removal is assessed at various intercalation conditions, including temperature  $T$  ( $^\circ\text{C}$ ), time  $t$  (h), and CTAB loading  $m_c$  (% w/w). The three independent variables are optimized using Minitab version 18.1. The detailed interlayer structure of CTAB@Bent and its surface interaction with  $\beta$ -carotene from CPO are observed, with properties such as the cation exchange capacity (CEC) of CTAB@Bent,  $\beta$ -carotene content, free fatty acid (FFA) content, and peroxide value (PV) of CPO being monitored.

## 2. RESULTS AND DISCUSSIONS

### 2.1. Influence of the Intercalation Parameters on the Bleaching Performance of CTAB@Bent.

The interaction

between the two intercalation parameters on the bleaching performance of CTAB@Bent is presented in Figure 1A.1–A.3. As seen from the figure, the intercalation temperature is the most significant variable affecting the bleaching performance of CTAB@Bent, subsequently followed by the CTAB loading and the intercalation time. Figure 1A.1,A.2 shows that the declining temperature of intercalation significantly escalates the bleaching ability of CTAB@Bent regardless of the other two parameters. This is likely because the higher the temperature, the more saturated the surface of CTAB@Bent, thus providing fewer adsorption sites to capture  $\beta$ -carotene.<sup>19</sup> A higher intercalation temperature induces a forthright migration of surface cation from bentonite, which leaves bentonite with a negative charge. This provokes the cationic CTAB to interact with bentonite to balance the surface charge. The interaction between them leads to the intercalation of CTAB into the bentonite layer,<sup>16,20</sup> where the hydrophilic heads of CTAB attach to the silicon tetrahedral surface of bentonite, and, at the same time, the hydrophobic tails interact with each other to widen the interlayer spacing of bentonite.<sup>21</sup> However, a larger number of positively charged CTAB heads linked to the bentonite surface at a higher temperature result in the formation of denser hydrophobic tails in the interlayer region, which consequently cover the active sites of bentonite and lower its ability to adsorb  $\beta$ -carotene.

Figure 1A.2–A.3 presents the effect of the CTAB loading on the bleaching performance of CTAB@Bent. As the surfactant loading increases from  $m_c = 0.20$  to 0.33% (w/w), the adsorption efficiency of CTAB@Bent toward  $\beta$ -carotene also significantly escalates. However, with a further rise to  $m_c = 1.00\%$  (w/w), the removal rate of  $\beta$ -carotene reached a plateau point. At the lower amount of CTAB, the better bleaching performance can be attributed to the effective interaction between the unoccupied sites in the surface of the clay and the cationic head of the long-tailed CTAB to form a hemi-micellar layer. Moreover, the easier mobility onto the interlayer region also consecutively induces the occurrence of hydrophobic binding between intercalated bentonite and  $\beta$ -carotene in CPO. Meanwhile, a further increase of CTAB loading causes surface saturation due to ion pairing<sup>19</sup> and the formation of a admicellar region that is a result of the hydrophobic interaction between the tail of intercalated CTAB and the tail of the free CTAB ion (CTA<sup>+</sup>).<sup>19,22,23</sup> This results in lower active sites that are available for the adsorption of the unwanted components in CPO.

The influence of time during intercalation was investigated at three different levels ( $t = 2, 4,$  and 6 h). Figure 1A.1,A.3 shows a gradual increase of the  $\beta$ -carotene removal rate when the time is extended from  $t = 2$  to 4 h, and further prolonging the intercalation time to the highest level ( $t = 6$  h), on the other hand, slightly reduces the  $\beta$ -carotene removal rate. Allowing longer contact between CTAB solution and bentonite ensures that more cationic CTA<sup>+</sup> intercalated into the silicate layers. However, a longer duration causes surface saturation and a clustered interlayer spacing that lowers the number of adsorption sites, therefore leading to a lower removal rate.

An inverse correlation between the CEC value of CTAB@Bent and the removal rate of  $\beta$ -carotene in various intercalation parameters is observed and is depicted in Figure 2A–C. The removal rate of  $\beta$ -carotene decreases from 70.22 to 55.93% (w/w) when the intercalation temperature rises from  $T = 40$  to 60 °C at a constant  $t = 4$  h and  $m_c = 1.00\%$  (w/w), while the

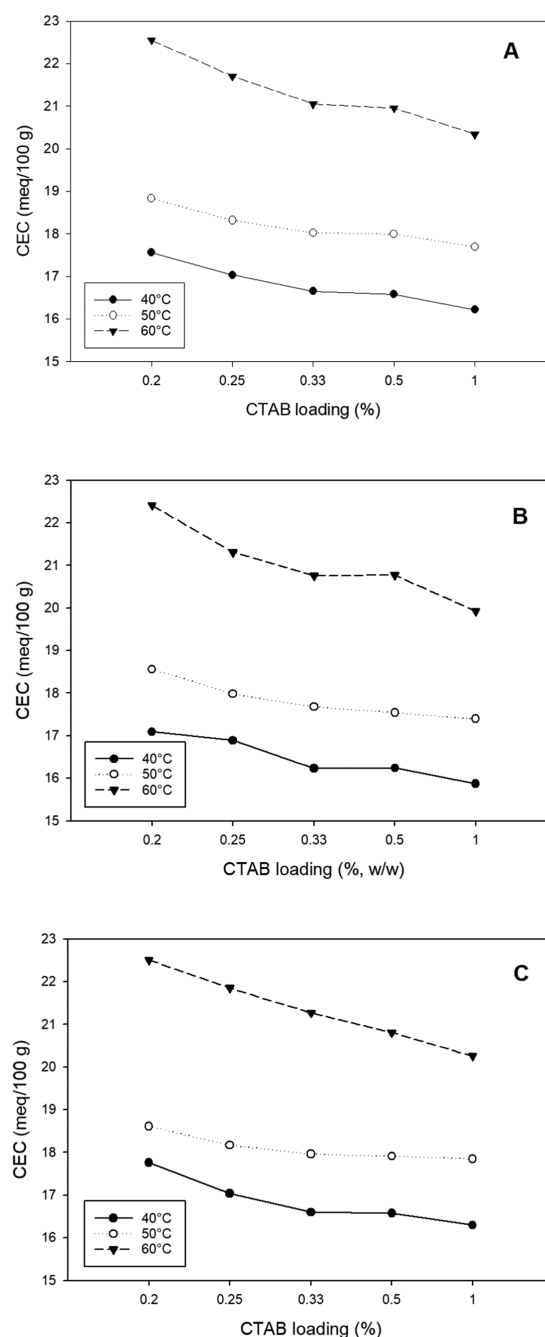


**Figure 2.** Effect of CTAB loading  $m_c$  (% w/w) and temperature  $T$  (°C) on the CEC value of CTAB@Bent at three different intercalation times: (A)  $t = 2$  h, (B)  $t = 4$  h, and (C)  $t = 6$  h.

CEC value escalates from 15.87 to 19.92 mequiv/100 g. The CEC value also slightly decreases as the amount of CTAB is enhanced, and, at the same time, only a slight difference of CEC is observed within the tested range of the intercalation time. It is notable that temperature is the primary cause in the alteration of CEC values, where a higher temperature induces cation removal from the bentonite surface, leading to a higher concentration of CTA<sup>+</sup> linked to its surface, which subsequently increases the number of exchangeable cations, implied by the CEC value. The CEC values of all CTAB@Bent samples are monitored to be lower than the original CEC value of R-Bent, further emphasizing the role of CTAB in the change of the CEC value and the removal rate of  $\beta$ -carotene. As a

lower CEC value directly indicates a better  $\beta$ -carotene removal ability, the CEC value can be considered as a prominent and simple indicator to estimate the ability of CTAB@Bent to remove  $\beta$ -carotene.

**2.2. Optimization Study.** In this study, MLFD-based RSM was employed to determine the optimum conditions for the bentonite modification using CTAB by simultaneously incorporating three important variables (temperature  $T$ , time  $t$ , and CTAB loading  $m_c$ ). The correlation between the responses and the series of coded input variables is presented in Table 1. Using the least-squares analysis (performed by Minitab version 18.1), the second-order polynomial equation (eq 1) was found to be the best-fitted model to represent the experimental data.

$$\begin{aligned} \beta - \text{carotene removal rate}(\%, \text{ w/w}), Y \\ = 65.13 - 19.67(T) + 11.54(t) + 3.455(m_c) \\ + 3.306(T^2) - 3.442(t^2) - 0.1596(m_c^2) \\ + 0.407(T)(t) - 0.142(T)(m_c) - 0.167(t)(m_c) \end{aligned} \quad (1)$$

where  $Y$  is the removal rate of  $\beta$ -carotene (% w/w) and  $T$ ,  $t$ , and  $m_c$  are the coded levels of the independent variables (1, 2, and 3 for  $T$  and  $t$  and 1, 2, 3, 4, and 5 for  $m_c$ ).

The mathematical model above shows that  $t$ ,  $m_c$ ,  $T^2$ , and  $(T)(t)$  have a favorable influence on the increase of  $\beta$ -carotene removal rate, while the negative coefficients of  $T$ ,  $t^2$ ,  $m_c^2$ ,  $(T)(m_c)$ , and  $(t)(m_c)$  indicate that the increase of these variables decreases the response. A significant study of the three independent variables performed by statistical ANOVA is presented in Table 2. The model suggests that all terms except the quadratic CTAB loading ( $m_c^2$ ) and the two-way interactions ( $p$ -value > 0.05) are prominent. The Pareto chart of standardized effect (Figure 3) also shows that all of the first-order terms are notable with the significance order as follows: temperature  $T$  > CTAB loading  $m_c$  > time  $t$ .

The  $R$ -squared of the coded model (eq 1) is obtained at 0.9819, pointing that 98.19% of the experimental results can be closely interpreted by the quadratic equation above. The values of adjusted and predicted  $R$ -squared that are close to unity (0.9773 and 0.9689, respectively) also indicate that the predicted and actual removal rates of  $\beta$ -carotene conform to each other. Therefore, the regressed mathematical model is considered adequate to define the behavior of all independent input variables.

Figure 1B.1–B.3 depicts the influence of two independent design variables on the profile of the predicted response. It can be seen that the escalating temperature from the lowest to the highest level has a significant antagonistic influence on the response, and, conversely, the removal rate of  $\beta$ -carotene gradually increases along with the enhancement of CTAB loading from  $m_c = 0.2$  to 0.33% (w/w). A further increase to  $m_c = 1.00\%$  (w/w) insignificantly improves its removal rate. Only a slight increase in the removal rate of  $\beta$ -carotene is observed when time is extended from the bottom level to the middle one, while a further time extension to the highest level results in a lower  $\beta$ -carotene removal rate. The profiles are in agreement with the Pareto chart presented in Figure 3, where it is evident that intercalation temperature is the most significant variable affecting the removal rate of  $\beta$ -carotene, subsequently followed by the CTAB loading and intercalation time.

The optimized intercalation conditions to obtain the highest removal rate of  $\beta$ -carotene are generated using Minitab

**Table 1. Experimental Design Matrix Based on MLFD Along with the Experimental and Predicted Response ( $\beta$ -Carotene Removal, %, w/w)**

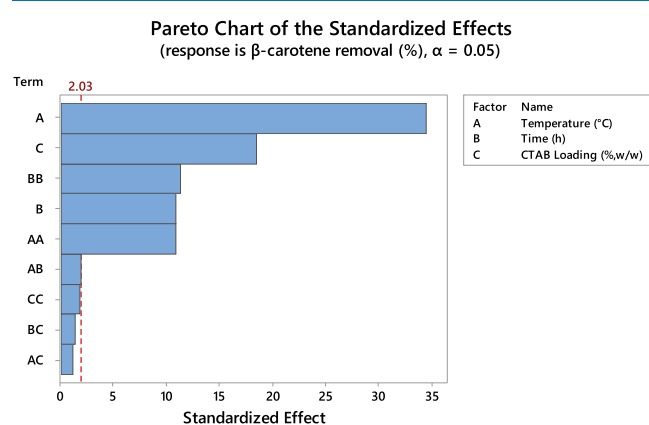
run	sample code (CTAB@Bent-)	$T$	$t$	$m_c$	response ( $\beta$ -carotene removal, %, w/w)	
					experimental ( $n = 3$ ) <sup>a</sup>	predicted <sup>a</sup>
1	231	2	3	1	47.55	47.61
2	114	1	1	4	66.59	67.30
3	332	3	3	2	47.63	47.60
4	311	3	1	1	48.65	47.90
5	235	2	3	5	55.23	54.46
6	335	3	3	5	51.39	51.83
7	222	2	2	2	53.81	54.99
8	315	3	1	5	55.69	55.51
9	214	2	1	4	57.95	57.39
10	224	2	2	4	59.11	58.75
11	121	1	2	1	63.07	61.71
12	334	3	3	4	49.92	50.74
13	211	2	1	1	50.08	50.77
14	122	1	2	2	65.31	64.21
15	322	3	2	2	51.72	52.38
16	134	1	3	4	61.05	62.32
17	223	2	2	3	56.93	57.03
18	213	2	1	3	55.86	55.50
19	124	1	2	4	66.92	68.25
20	132	1	3	2	59.44	58.61
21	113	1	1	3	66.46	65.27
22	111	1	1	1	60.43	60.26
23	221	2	2	1	52.19	52.63
24	115	1	1	5	67.65	69.01
25	321	3	2	1	50.02	50.16
26	225	2	2	5	61.68	60.15
27	135	1	3	5	63.92	63.70
28	123	1	2	3	66.79	66.39
29	331	3	3	1	46.79	45.55
30	131	1	3	1	54.76	56.28
31	125	1	2	5	70.22	69.80
32	312	3	1	2	49.73	50.28
33	133	1	3	3	60.81	60.63
34	233	2	3	3	52.08	51.67
35	313	3	1	3	53.55	52.34
36	215	2	1	5	59.49	58.96
37	325	3	2	5	55.93	57.11
38	324	3	2	4	55.16	55.85
39	232	2	3	2	48.92	49.80
40	333	3	3	3	49.80	49.33
41	323	3	2	3	54.68	54.28
42	234	2	3	4	53.90	53.22
43	314	3	1	4	54.08	54.09
44	112	1	1	2	63.15	62.92
45	212	2	1	2	51.28	53.30

<sup>a</sup>The standard error of estimate (SEE) between the experimental and predicted responses was 0.67%.

(version 18.1) and acquired at  $T = 40$  °C,  $t = 3.2$  h, and  $m_c = 1.00\%$  (w/w), with the predicted response of 70.30% (w/w) and model desirability of 1.0 (Figure 4). The model reliability is verified by performing three replicated bleaching experiments using CTAB@Bent obtained at optimum intercalation conditions (CTAB@Bent-Opt) as the adsorbent. The average removal rate of  $\beta$ -carotene is monitored at 71.04% (w/w).

**Table 2. Significance Study of Various Tested Variables for Response Calculation Performed by ANOVA**

term	coefficient	SE coefficient	T-value	P-value
constant	57.018	0.364	156.46	0.000
$T$	-6.061	0.176	-34.43	0.000
$t$	-1.915	0.176	-10.88	0.000
$m_c$	3.756	0.203	18.48	0.000
$T^2$	3.306	0.305	10.84	0.000
$t^2$	-3.442	0.305	-11.29	0.000
$m_c^2$	-0.638	0.344	-1.86	0.072
$(T)(t)$	0.407	0.216	1.89	0.068
$(T)(m_c)$	-0.285	0.249	-1.14	0.261
$(t)(m_c)$	-0.335	0.249	-1.34	0.187
R-squared ( $R^2$ )			0.9819	
adjusted $R^2$			0.9773	
predicted $R^2$			0.9689	

**Figure 3.** Significance order of the three tested variables (intercalation temperature  $T$  (A), time  $t$  (B), and CTAB loading  $m_c$  (C)) on the  $\beta$ -carotene removal, as shown by the Pareto chart of the standardized effect.

With an error of only 0.74% between the predicted and experimental results, we can conclude that the established mathematical model is highly reliable and provides sufficient accuracy for predicting  $\beta$ -carotene removal efficiency within the tested intercalation levels. From an industrial viewpoint, a low temperature ( $T = 40$  °C) and a relatively short duration ( $t = 3.2$  h) are generally favorable since they provide beneficial support in increasing the production efficiency.

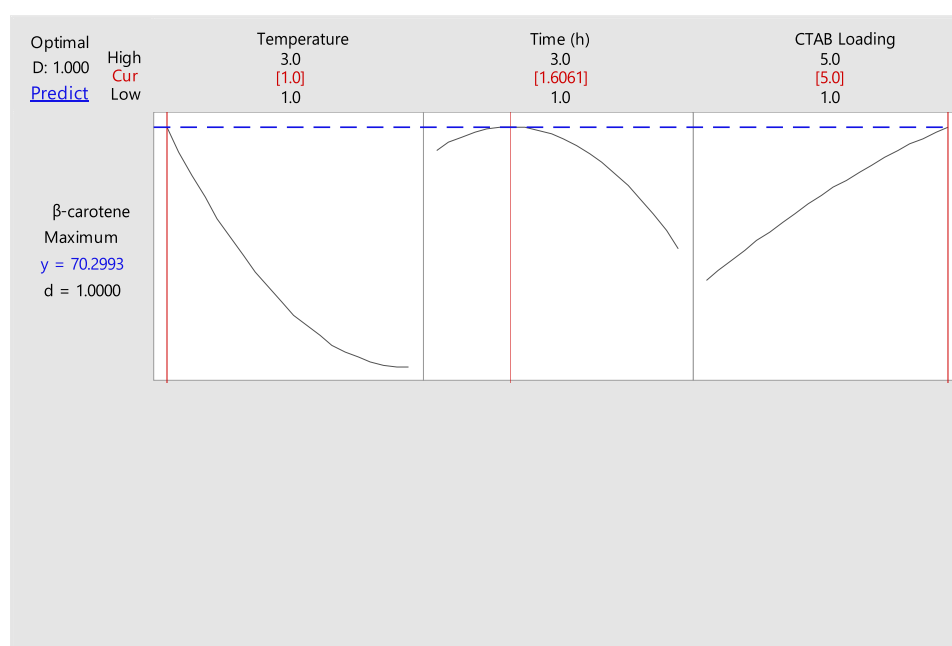
### 2.3. Comparative Study of the Bleaching Performance among CTAB@Bent-Opt, R-Bent, and Acid-Activated Bentonite (Acid-Bent). Table 3 summarizes the

**Table 3. Characteristics of Raw Materials**

parameters	result
CPO	
$\beta$ -carotene content, ppm	808.13
FFA, % (w/w)	4.20
PV, mequiv/kg	2.76
R-Bent	
CEC, mequiv/100 g	28.42

characteristics of R-Bent and CPO as the raw material for the bleaching process; meanwhile, the CEC of the prepared bentonites (CTAB@Bent-Opt, R-Bent, and Acid-Bent) are depicted in Figure 5. The Acid-Bent was prepared following the method reported by Fabryanty et al.:<sup>24</sup> bentonite was soaked for 2 h at 60 °C in 5 N sulfuric acid solution. The bleaching performances of CTAB@Bent-Opt, R-Bent, and Acid-Bent are evaluated from the decrease of FFA, PV, and  $\beta$ -carotene content in CPO.

As shown in Table 4, CTAB@Bent-Opt reduces a higher content of  $\beta$ -carotene than R-Bent and Acid-Bent. CTAB@Bent-Opt can remove 71.04% (w/w)  $\beta$ -carotene from CPO, while R-Bent and Acid-Bent can achieve only a 16.93% and 41.45% (w/w) removal rate, respectively. This is attributed to the increased hydrophobicity of the bentonite surface caused by the presence of the hydrophobic tail of the intercalated

**Figure 4.** Optimization plot of the intercalation parameters.

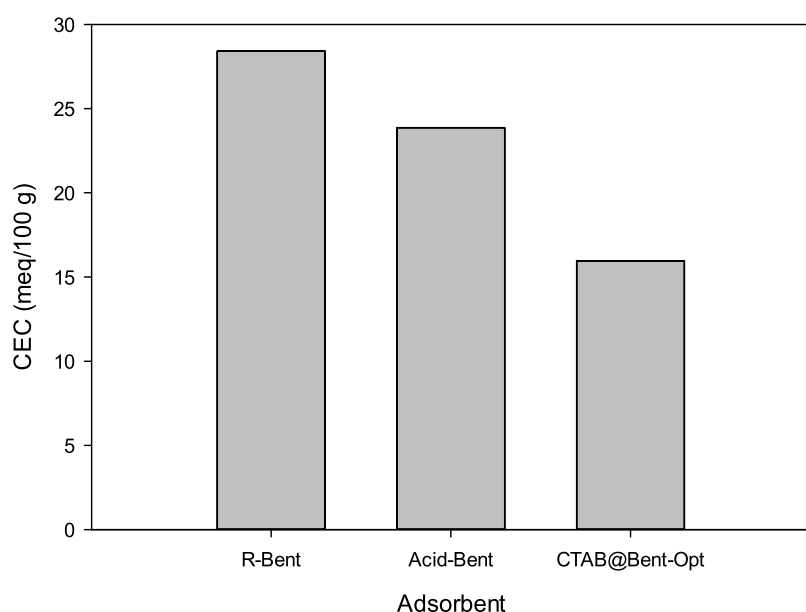


**Figure 5.** CEC values of three different adsorbents (R-Bent, Acid-Bent, and CTAB@Bent-Opt).

**Table 4. Important Parameters of CPO after Adsorption with Various Types of Adsorbents**

parameters	characteristic of CPO after adsorption with		
	R-Bent	Acid-Bent	CTAB@Bent-Opt
$\beta$ -carotene removal rate (% w/w)	16.93	41.45	71.04
FFA (% w/w)	4.25	4.42	4.03
PV (mequiv/kg)	2.88	4.92	3.12

CTAB, which is favorable for binding  $\beta$ -carotene. Fiedor and Burda also mentioned that one of  $\beta$ -carotene's characteristics is that the compound can act as an anti- and pro-oxidant.<sup>25</sup> Therefore,  $\beta$ -carotene can spontaneously react with the peroxy radical ions in CPO (as indicated by PV) at a high temperature to form the unstable oxidized carotenes, which promote the interaction with CTAB to stabilize the degraded chain (Figure 6).<sup>25,26</sup>

The FFA content in CPO decreases after adsorption with CTAB@Bent-Opt, while it slightly increases for the other two adsorbents (R-Bent and Acid-Bent). It can, however, be neglected since the difference is insignificant. In the case of PV, a steady increase is observed in CPO after adsorption with the order (from the lowest to the highest) of R-Bent, CTAB@Bent-Opt, and Acid-Bent. Figure 5 shows that R-Bent has the highest CEC value (28.42 mequiv/100 g), followed by Acid-Bent and CTAB@Bent-Opt (23.87 and 15.96 mequiv/100 g, respectively). A negative correlation between the CEC value and the removal rate of  $\beta$ -carotene is also observed in this comparative study. The removal rate of  $\beta$ -carotene goes up from 16.93 to 71.04% (w/w) when the CEC value declines from 28.42 to 15.96 mequiv/100 g. This occurrence further proves that CEC is a significant parameter to determine the removal rate of  $\beta$ -carotene.

**2.4. Characterization of CTAB@Bent-Opt.** Figure 7A,B depicts the surface morphologies of R-Bent and CTAB@Bent-Opt, respectively. Both figures present no significant difference in the surface morphology of both materials, indicating that the intercalation of CTAB into the interlayer spacing of R-Bent

does not alter its macroscopic characteristics. Meanwhile, the FTIR spectra (Figure 7C) show that the fingerprint functional groups of CTAB, e.g., ammonium moiety band ( $3419\text{ cm}^{-1}$ ), C–H vibration bands of  $-\text{CH}_2$  ( $2914\text{--}2864\text{ cm}^{-1}$ ), stretching vibration band of  $\text{N}^+\text{--CH}_3$  (asymmetric vibration band at  $1665\text{ cm}^{-1}$  and symmetric vibration band at  $1470\text{ cm}^{-1}$ ),  $-\text{CH}_3$  vibration band ( $950\text{ cm}^{-1}$ ), and  $\text{Br}^-$  band ( $714\text{ cm}^{-1}$ ), are found in CTAB@Bent-Opt, implying that the cationic surfactant is successfully intercalated into the bentonite interlayer surface.

Figure 7D shows the nitrogen sorption isotherm analysis of CTAB@Bent-Opt. According to the IUPAC classification, CTAB@Bent-Opt exhibits a type I isotherm with the hysteresis loop-type  $\text{H}_3$ , which is the characteristic of the microporous structure. This type of hysteresis loop indicates that the solid is built of particle aggregates that form very complex and nonuniform pores, with slit shapes or plates.<sup>27</sup> The major textural properties of R-Bent and CTAB@Bent-Opt are obtained from the BET isotherm. While the specific surface area and pore volume of R-Bent are found to be  $51\text{ m}^2/\text{g}$  and  $0.093\text{ cm}^3/\text{g}$ , respectively, the corresponding values of both parameters for CTAB@Bent-Opt are  $121\text{ m}^2/\text{g}$  and  $0.214\text{ cm}^3/\text{g}$ . The increased specific surface area and pore volume can be explained by the expansion of the lamellar spacing between the sheets.<sup>28,29</sup>

R-Bent and CTAB@Bent-Opt are further analyzed by XRD, and their patterns are shown in Figure 7E along with their basal spacing  $d(001)$  values. A higher basal spacing is obtained for CTAB@Bent-Opt ( $25.1\text{ \AA}$ ) than for R-Bent ( $12.7\text{ \AA}$ ), due to the intercalation of CTAB in bentonite.<sup>13,30</sup> As also stated in the nitrogen sorption isotherm analysis, the XRD results further verify that the pore volume enlargement occurs during the synthesis of CTAB@Bent-Opt.

**2.5. Isotherm Study of the Bleaching Process Using CTAB@Bent-Opt.** To study the mechanism of the bleaching process using CTAB@Bent-Opt, three isotherm equations (Freundlich, Dubinin–Radushkevich (D–R), and Langmuir) are fitted into the equilibrium data at different temperatures (Table 5). The developed isotherms at a temperature of  $100\text{ }^\circ\text{C}$  are plotted in Figure 8. The Freundlich constant ( $K_F$ ) and

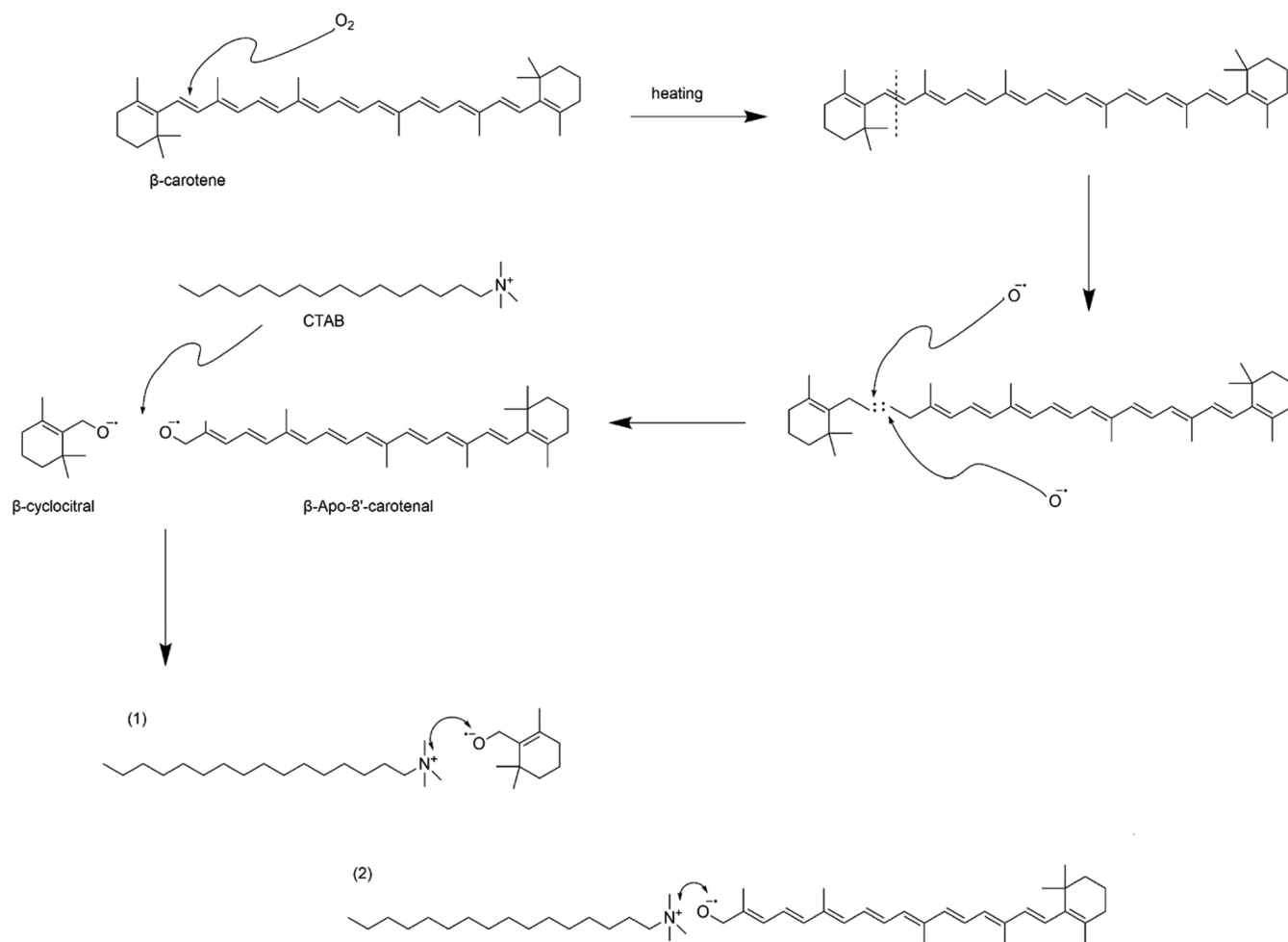


**Figure 6.** Schematic diagram of  $\beta$ -carotene oxidation and its ion-exchange interaction with the cationic head of CTAB.

$1/n$  are obtained from the nonlinear regression between  $C_e$  and  $Q_e$ . Table 5 shows that the value of  $1/n$  ranges from 0.336 to 0.489. The  $1/n$  value measures the adsorption favorability, with less than 1 representing favorable adsorption.<sup>31</sup> Meanwhile, the Freundlich constant ( $K_F$ ) increases significantly when the temperature escalates from 80 to 100 °C, with a further increase to 120 °C giving a slightly lower value of  $K_F$ , indicating that the adsorption of  $\beta$ -carotene onto the surface of CTAB@Bent-Opt is an endothermic process. Further analysis using the Langmuir model gives similar results. The value of the Langmuir constant ( $K_L$ ) sharply escalates from 0.0026 to 0.0070 L/mg as the temperature rises from 80 to 120 °C, emphasizing that the process is favorable at higher temperatures and certainly endothermic. The calculated  $Q_{m(L)}$  is found to be increased along with the temperature, from 29.42 mg/g at 80 °C to 37.80 mg/g at 120 °C.

Another isotherm studied in this work is the Dubinin–Radushkevich model. This model determines the adsorption nature of CTAB@Bent-Opt toward  $\beta$ -carotene by calculating the mean sorption energy ( $E$ ), which is defined as the free energy transfer of 1 mol of solute from the infinity of the surface of the adsorbent. The correlation between the D–R isotherm and mean energy sorption ( $E$ ) can be expressed by the equation below

$$E = \frac{1}{\sqrt{2\beta}} \quad (2)$$

where  $E$  is the mean energy sorption (kJ/mol) and  $\beta$  is the constant of D–R isotherm ( $\text{mmol}^2/\text{J}^2$ ). Mean sorption energy provides information about the adsorption mechanism, where a value between 8 and 16 kJ/mol indicates that the sorption is chemisorption, while the sorption is supposed to occur via physical interaction when the mean sorption energy is lower than 8 kJ/mol.<sup>32</sup> The magnitude of  $E$  is obtained at a value lower than 8 kJ/mol for all tested temperatures, indicating that the major governing mechanism of this adsorption is physical binding. However, as depicted in Figure 6, our study also suggests that there is a minor interaction between the oxidized  $\beta$ -carotene with the cationic head of CTAB through the ion-exchange mechanism.

The goodness of the fit of the isotherm models is analyzed using the correlation coefficient ( $r^2$ ) and reduced chi-square ( $\chi^2$ ) (Table 5). Based on the equilibrium data, the  $\beta$ -carotene adsorption onto CTAB@Bent-Opt is best-fitted to the D–R isotherm model and majorly driven by physical adsorption. The overall experimental data also show that CTAB@Bent-Opt possesses a high affinity toward  $\beta$ -carotene and is a potential adsorbent for the bleaching process of CPO.

Table 6 summarizes the thermodynamic parameters of the adsorption of  $\beta$ -carotene onto the surface of CTAB@Bent-Opt. Three important parameters, e.g., Gibbs free energy change ( $\Delta G^\circ$ ), enthalpy ( $\Delta H^\circ$ ), and entropy ( $\Delta S^\circ$ ), are investigated. Negative values of Gibbs free energy ( $\Delta G^\circ$ ) verify the spontaneous (favorable) adsorption of  $\beta$ -carotene, and its

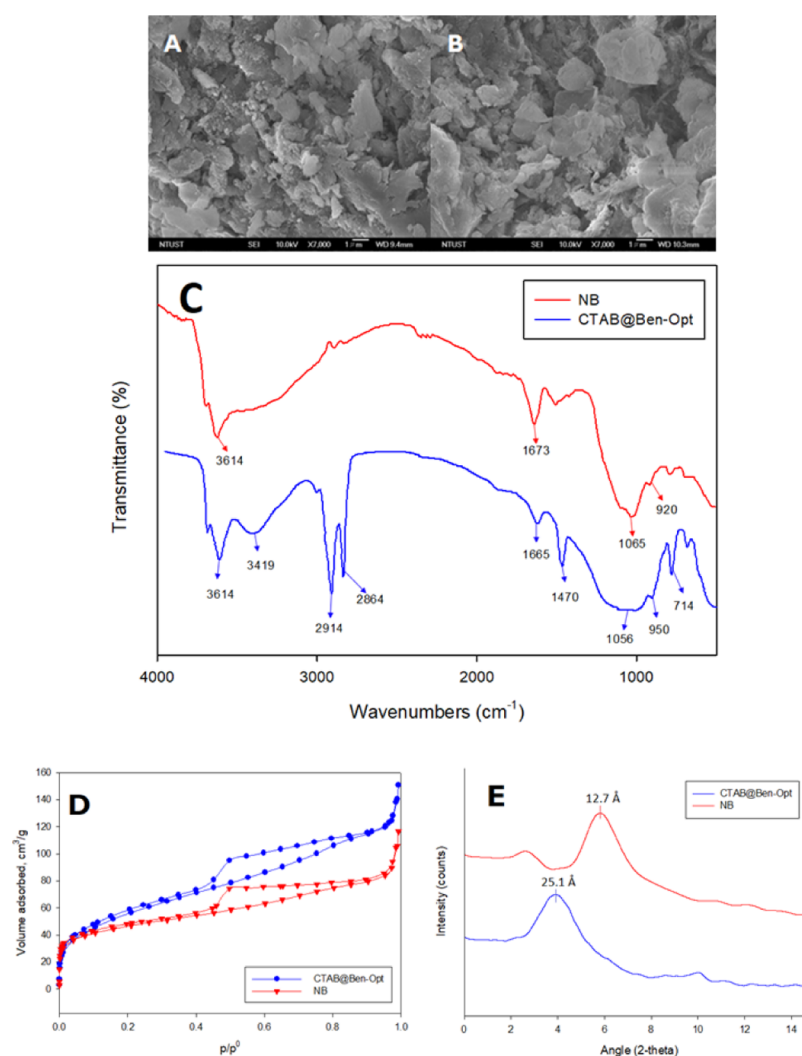


**Figure 7.** SEM images of (A) R-Bent and (B) CTAB@Bent-Opt and (C) FTIR spectra, (D) nitrogen sorption analysis, and (E) XRD patterns for R-Bent and CTAB@Bent-Opt.

**Table 5. Parameters of the Fitted Isotherms for the Adsorption of  $\beta$ -Carotene onto the CTAB@Bent-Opt Surface**

isotherm	parameters	temperature (K)		
		353	373	393
Freundlich	$K_F$ ((mg/g) (L/mg) <sup>1/n</sup> )	0.86	2.83	2.63
	$1/n$	0.489	0.336	0.394
	$r^2$	0.8094	0.8101	0.9548
	$\chi^2$	2.9511	3.8614	2.1180
Langmuir	$Q_{m(L)}$ (mg/g)	29.42	32.65	37.80
	$K_L$ (L/mg)	0.0026	0.0069	0.0070
	$r^2$	0.8536	0.8830	0.9813
	$\chi^2$	2.2664	2.3791	0.877
Dubinin–Radushkevich	$Q_{m(D-R)}$ (mg/g)	21.95	23.57	28.25
	$E$ (kJ/mol)	0.015	0.029	0.040
	$r^2$	0.9534	0.9787	0.9635
	$\chi^2$	0.7212	0.4335	1.7084

escalating values along with the temperature imply that a higher temperature results in a higher affinity of  $\beta$ -carotene toward CTAB-Ben@Opt. The enthalpy of the adsorption is found to be positive (28.088 kJ/mol), confirming the adsorption endothermic nature, while the absolute value of  $\Delta S^\circ$  (141.1 J/(mol·K)) indicates the affinity of the adsorbate ( $\beta$ -carotene) toward the sorbent (CTAB@Bent-Opt).<sup>33</sup>

**2.6. Mechanism Study of  $\beta$ -Carotene Adsorption onto the Surface of CTAB@Bent-Opt.** Using the surface property data of the adsorbent, the adsorption isotherm, and thermodynamic results, the adsorption mechanism is studied to illustrate the interaction between  $\beta$ -carotene as the adsorbate and CTAB@Bent-Opt as the adsorbent. The CTAB@Bent-Opt molecules are constructed by the negative-

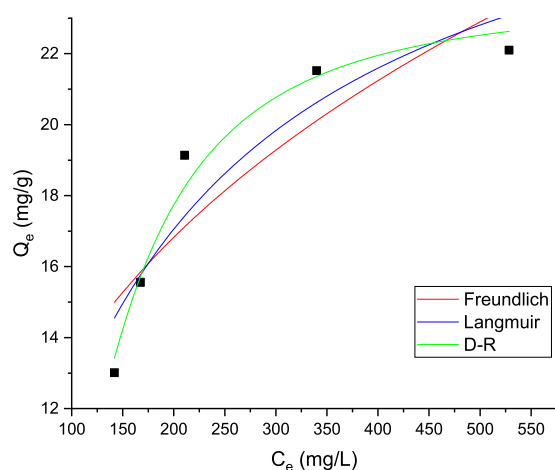


**Figure 8.** Fitted isotherm profiles for the equilibrium data of CPO bleaching using CTAB@Bent-Opt (bleaching temperature = 100 °C, time = 1 h, agitation speed = 250 rpm).

**Table 6. Thermodynamic Parameters of the Adsorption of  $\beta$ -Carotene onto the Surface of CTAB@Bent-Opt**

temperature (K)	thermodynamic parameters		
	$\Delta G^\circ$ (kJ/mol)	$\Delta H^\circ$ (kJ/mol)	$\Delta S^\circ$ (J/(mol·K))
353	-21.25	28.088	141.1
373	-25.48		
393	-26.90		

charge bentonites (one layer of bentonite consists of two tetrahedral silica sheets and one sheet of aluminum octahedral) and a substantial amount of CTAB intercalated in the interlayer of bentonite to form a hydrophobic surface with a higher basal spacing, as presented in Figure 9. Meanwhile,  $\beta$ -carotene is biochemically synthesized from eight isoprenes and

contains a 40-carbon chain; therefore, it is extremely hydrophobic.

Based on the isotherm and thermodynamic study, the removal of  $\beta$ -carotene is greatly affected by temperature, as evident from the significant increase of the  $\beta$ -carotene removal rate along with the temperature rise. Moreover, as mentioned above, the major mechanism governing the adsorption is physical attraction. Therefore, according to our findings, the mechanism of  $\beta$ -carotene adsorption onto the CTAB@Bent-Opt surface can be assumed to follow these steps:

- Migratory movement of  $\beta$ -carotene from the CPO bulk onto the boundary layer of CTAB@Bent-Opt.
- The heavily polar bonded water molecules retained on the CTAB@Bent-Opt surface are associated with the water molecules from the CPO and increase the water entropy. As the randomness of the adsorbent–adsorbate association increases, it gives an opportunity for  $\beta$ -carotene to diffuse and pass through the boundary layer of CTAB@Bent-Opt into the hydrophobic interlayer.
- $\beta$ -Carotene adsorption on the hydrophobic interlayer surface of CTAB@Bent-Opt may be caused by the physical interaction and the ion-exchange interaction between oxidized  $\beta$ -carotene and CTA<sup>+</sup>, as implied in Figure 10.

### 3. CONCLUSIONS

The intercalation of CTAB into the bentonite interlayer has been successfully employed to enhance the hydrophobicity and adsorption capacity of bentonite toward  $\beta$ -carotene. All intercalation parameters significantly influence the removal rate of  $\beta$ -carotene, with the following order: temperature  $T >$  CTAB loading  $m_c >$  time  $t$ . The maximum  $\beta$ -carotene removal rate using CTAB@Bent-Opt (obtained at  $T = 40$  °C,  $t = 3.2$  h and  $m_c = 1.00\%$  (w/w)) is 71.04% (w/w), higher than those

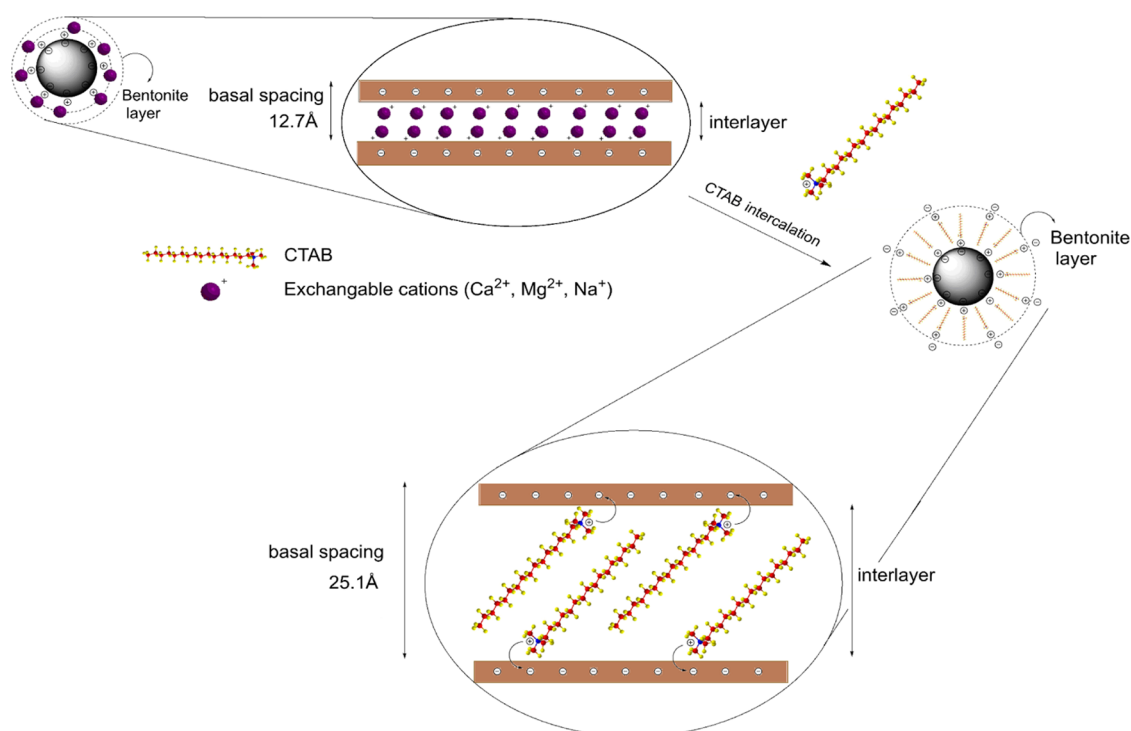


**Figure 9.** Intercalation mechanism of CTAB into the interlayer of R-Bent.

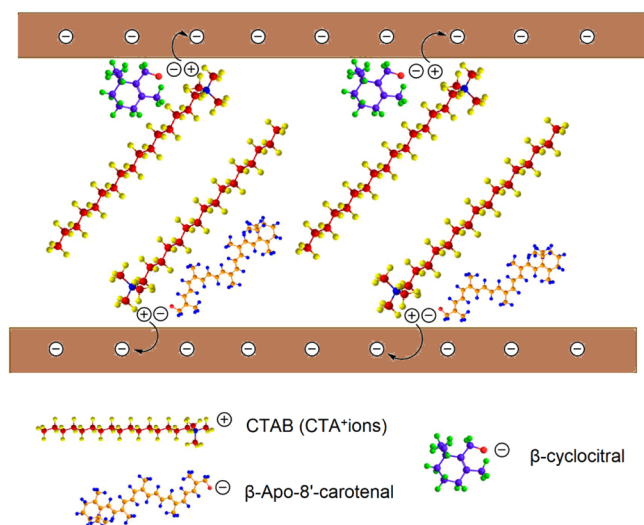


**Figure 10.** Illustration of  $\beta$ -carotene adsorption onto the interlayer of CTAB@Bent-Opt, where  $\beta$ -Apo-8'-carotenal and  $\beta$ -cyclocitral are the breakdown products of  $\beta$ -carotene due to oxidation.

using R-Bent and Acid-Bent, indicating that CTAB@Bent-Opt possesses a greater affinity toward  $\beta$ -carotene than the other two conventional bleaching agents. This  $\beta$ -carotene removal rate is also found to be significantly higher (more than two-fold) than that reported in the previous study by Gunawan et al.,<sup>13</sup> which is likely attributed to the optimization approach carried out in this study. The adsorption process is endothermic, spontaneous, and may be driven by physical attraction and a minor interaction between  $\beta$ -carotene and  $\text{CTA}^+$ .

## 4. MATERIALS AND METHODS

**4.1. Materials.** Raw bentonite (R-Bent) was collected from Pacitan, East Java, Indonesia. It was pulverized to fine particles (100–150  $\mu\text{m}$ ) before being subjected to organic impurities' removal by soaking the particles in a 30% (w/w) hydrogen peroxide solution for 3 h at room temperature. The treated R-Bent was subsequently washed with deionized water, dried overnight at 110  $^{\circ}\text{C}$  to remove the excess water, and repulverized to particles with a size of 100–150  $\mu\text{m}$ . Meanwhile, CPO was obtained from the local industry in Gresik, Indonesia. Prior use, CPO was degummed using 0.1% (w/w) phosphoric acid (85% purity) to dissociate the phospholipids and gums into phosphatidic acid, which can be easily removed during the bleaching process. The degumming process was performed at a temperature of 90  $^{\circ}\text{C}$  for 2 h. Several important characteristics of CPO, e.g., FFA, PV, and  $\beta$ -carotene content, were analyzed in accordance with the standard methods of AOCS Ca 5a-40, AOCS Cd 8b-90, and Speck et al.,<sup>34</sup> respectively; the CEC of R-Bent was measured using ASTM C837-99. The characteristics of both raw materials are presented in Table 3. CTAB as the intercalating agent, sulfuric acid ( $\text{H}_2\text{SO}_4$ , 95–98% purity), and methylene blue were purchased from Merck (Merck, Germany). All chemicals and reagents used in the analysis were of analytical grade and required no further purification.

**4.2. Statistical Experimental Design and Process Optimization of CTAB Intercalation into R-Bent.** The combination of multilevel factorial design (MLFD) and response surface methodology (RSM) was statistically

employed to obtain the optimum intercalation condition that gives the highest removal of  $\beta$ -carotene. Based on their industrial relevance, three independent variables were selected as critical parameters, including intercalation temperature  $T$  ( $^{\circ}\text{C}$ ), time  $t$  (h), and CTAB loading  $m_c$  (% w/w). As material costs generally pose as the major operating expense,<sup>35,36</sup> CTAB loading is encoded into five different levels with 1 as the lowest and 5 as the highest level to closely monitor its influence on the removal rate of  $\beta$ -carotene. Meanwhile, the other two variables are divided into three levels: low (1), middle (2), and high (3). Table 7 presents the coded variables corresponding to their actual values.

**Table 7. Coded Levels of the Three Independent Variables for the CTAB Intercalation into R-Bent**

variables	encoded factor	factor level				
		1	2	3		
temperature ( $^{\circ}\text{C}$ )	$T$	40	50	60		
time (h)	$t$	2	4	6		
CTAB loading (% w/w)	$m_c$	0.2	0.25	0.33	0.50	1.00

Table 1 summarizes the MLFD-based design of the experiment for various intercalation variables, the sample code of CTAB@Bent, and the experimental and predicted removal rates of  $\beta$ -carotene as the response. To obtain well-founded data reproducibility, all experimental runs were performed in triplicates and randomized order. The responses ( $Y$ ,  $\beta$ -carotene removal (% w/w)) were then fitted to the following quadratic equation using the analysis of variance (ANOVA) run by Minitab (version 18.1) with a 95% confidence level

$$Y = k_0 + \sum_{i=1}^i k_i X_i + \sum_{i=1}^i k_{ii} X_i^2 + \sum_{i=1}^i \sum_{j=1}^j k_{ij} X_i X_j \quad (3)$$

where  $Y$  is the predicted  $\beta$ -carotene removal rate (% w/w);  $k_0$ ,  $k_i$ ,  $k_{ii}$ , and  $k_{ij}$  are the coefficients for the intercept, linear, quadratic, and two-way interactions of the variables, respectively; and  $X_i$  and  $X_j$  are the encoded variables ( $A$ ,  $B$ , and  $C$ ). While the values of  $i$  and  $j$  vary from 1 to 3 for the intercalation temperature and time, they vary from 1 to 5 for CTAB loading. The  $R$ -squared ( $R^2$ ) of the regressed mathematical equation was used to evaluate the goodness of fit of the model to the experimental data. Three response surface plots were developed by maintaining one variable constant in the center point while manipulating the other two variables.

**4.3. Modification of R-Bent.** The treated R-Bent was modified by inserting CTAB into the silanol layers. Intercalation was performed by mixing 25 g of treated R-Bent with 250 mL of CTAB solution with various CTAB loadings ( $m_c = 0.20, 0.25, 0.33, 0.5, 1.00\%$  w/w). The modification of R-Bent was conducted at different temperatures ( $T = 40, 50, 60$   $^{\circ}\text{C}$ ) and time ( $t = 2, 4, 6$  h). After the modification process was complete, the solid phase was separated from the supernatant and repeatedly washed using deionized water. The solid was oven-dried at 110  $^{\circ}\text{C}$  overnight to obtain the CTAB@Bent particles. Modified CTAB@Bent was finally pulverized to 100–150  $\mu\text{m}$  sized particles prior to

use. The CEC value of every CTAB@Bent sample was also analyzed to observe its correlation with the modification variables.

**4.4. Bleaching Process of CPO.** The bleaching of CPO was conducted by adding 3% (w/w) of adsorbent to 100 g of degummed oil, which follows the industrial CPO refining steps. CPO was heated to 100 °C before the addition of the adsorbent. The solid–liquid mixture was then agitated at 250 rpm for 30 min at a constant temperature. After the desired time was reached, the bleached oil was separated from the adsorbent and collected for the analysis of  $\beta$ -carotene content. The removal rate of  $\beta$ -carotene content (% w/w) was calculated using the following equation

$$\beta - \text{carotene removal}(\%w/w) = \left( \frac{C_i - C_f}{C_i} \right) \times 100 \quad (4)$$

where  $C_i$  and  $C_f$  are the initial and final  $\beta$ -carotene concentrations in ppm, respectively. Meanwhile, FFA and PV were analyzed only for the bleached CPO with the highest  $\beta$ -carotene removal rate.

**4.5. Isotherm and Thermodynamic Studies of the Bleaching Process Using Optimized CTAB@Bent (CTAB@Bent-Opt).** The isotherm of  $\beta$ -carotene adsorption was conducted at temperatures of 80, 100, and 120 °C with various CTAB@Bent-Opt loadings,  $m_a$  ( $m_a = 1, 2, 3, 4,$  and 5% w/w). All experiments were carried out using the same procedure as explained in Section 4.4. The mass of the adsorbed  $\beta$ -carotene per unit mass of CTAB@Bent-Opt ( $Q_e$ ) at equilibrium was calculated by the following equation

$$Q_e(\text{mg/g}) = \frac{C_o - C_e}{m_a} \times V \quad (5)$$

where  $C_o$  and  $C_e$  are the initial and equilibrium concentrations of  $\beta$ -carotene in CPO (mg/L), respectively,  $m_a$  is the mass of CTAB@Bent-Opt (g), and  $V$  corresponds to the CPO volume (L).

The equilibrium data were fitted to several isotherm models (Langmuir, Freundlich, and Dubinin–Radushkevich (D–R)) and further analyzed to determine the thermodynamic parameters, e.g., Gibbs free energy ( $\Delta G^\circ$ ), enthalpy ( $\Delta H^\circ$ ), and entropy ( $\Delta S^\circ$ ), using eqs 6 and 7.

$$\Delta G^\circ = -RT \ln(K_L \cdot M_{\beta\text{-carotene}} \cdot 10^3 \cdot C^\circ) \quad (6)$$

$$\Delta G^\circ = \Delta H^\circ - T\Delta S^\circ \quad (7)$$

where  $R$  is the ideal gas constant (8.314 J/(mol·K)),  $T$  is the absolute temperature in Kelvin,  $K_L$  is an equilibrium constant of Langmuir isotherm in L/mg,  $M_{\beta\text{-carotene}}$  is the molar mass of  $\beta$ -carotene in g/mol, and  $C^\circ$  is the standard concentration in the reference state (1 mol/L).

**4.6. Characterization of CTAB@Bent-Opt.** The surface topography of CTAB@Bent-Opt was analyzed using SEM (JEOL JSM-6500F, Jeol Ltd., Japan) with an accelerating voltage of 10 kV and a 9.4–10.3 mm working distance, while its textural properties were measured using a Micromeritics ASAP 2010 sorption analyzer at 77 K. The XRD patterns of R-Bent and CTAB@Bent-Opt were acquired in the low-angle range ( $2\theta = 0\text{--}15^\circ$ ) using an X'PERT Panalytical Pro X-Ray diffractometer (Philips-FEL, the Netherlands, the wavelength of Cu  $K\alpha_1$  radiation ( $\lambda$ ) = 0.154 nm, voltage = 40 kV, tube current = 30 mA) to determine their basal spacings. Moreover, their functional groups were determined using FTIR analysis at

a wavenumber range of 4000–400  $\text{cm}^{-1}$  (Shimadzu FTIR 8400s).

## AUTHOR INFORMATION

### Corresponding Author

**Maria Yuliana** – Department of Chemical Engineering, Widya Mandala Catholic University Surabaya, Surabaya 60114, Indonesia; [orcid.org/0000-0002-3915-9401](https://orcid.org/0000-0002-3915-9401); Phone: (62) 31 3891264; Email: [maria\\_yuliana\\_liauw@yahoo.com](mailto:maria_yuliana_liauw@yahoo.com), [mariayuliana@ukwms.ac.id](mailto:mariayuliana@ukwms.ac.id); Fax: (62) 31 3891267

### Authors

**Revano J. Sutrisno** – Department of Chemical Engineering, Widya Mandala Catholic University Surabaya, Surabaya 60114, Indonesia

**Stefanus Hermanto** – Department of Chemical Engineering, Widya Mandala Catholic University Surabaya, Surabaya 60114, Indonesia

**Suryadi Ismadji** – Department of Chemical Engineering, Widya Mandala Catholic University Surabaya, Surabaya 60114, Indonesia; [orcid.org/0000-0002-5005-2824](https://orcid.org/0000-0002-5005-2824)

**Christian J. Wijaya** – Department of Chemical Engineering, Widya Mandala Catholic University Surabaya, Surabaya 60114, Indonesia; Department of Chemical Engineering, Faculty of Industrial Technology, Institut Teknologi Sepuluh Nopember, Surabaya 60111, Indonesia; [orcid.org/0000-0001-5679-3052](https://orcid.org/0000-0001-5679-3052)

**Shella P. Santoso** – Department of Chemical Engineering, Widya Mandala Catholic University Surabaya, Surabaya 60114, Indonesia; [orcid.org/0000-0003-4698-583X](https://orcid.org/0000-0003-4698-583X)

**Felycia E. Soetaredjo** – Department of Chemical Engineering, Widya Mandala Catholic University Surabaya, Surabaya 60114, Indonesia

**Yi-Hsu Ju** – Department of Chemical Engineering, Graduate Institute of Applied Science and Technology, and Taiwan Building Technology Center, National Taiwan University of Science and Technology, Taipei 10607, Taiwan

Complete contact information is available at: <https://pubs.acs.org/10.1021/acsoomega.0c04238>

### Author Contributions

The manuscript was written through the contributions of all authors. All authors have given approval to the final version of the manuscript.

### Notes

The authors declare no competing financial interest.

## ACKNOWLEDGMENTS

This research did not receive any specific grant from funding agencies in the public, commercial, or not-for-profit sectors.

## ABBREVIATION

CPO	crude palm oil
CTAB	cetyltrimethylammonium bromide
CTAB@Bent	CTAB-pillared bentonite
CTAB@Bent-Opt	optimized CTAB-pillared bentonite
R-Bent	raw bentonite
Acid-Bent	acid-activated bentonite
CEC	cation exchange capacity
FFA	free fatty acid
PV	peroxide value
MLFD	multilevel factorial design

RSM response surface methodology

## REFERENCES

- (1) USDA *Global Agricultural Information Network (GAIN)*, Indonesia Oilseeds and Products Annual 2019, 2019; pp 20.
- (2) Gibon, V.; De Greyt, W.; Kellens, M. Palm Oil Refining. *Eur. J. Lipid Sci. Technol.* **2007**, *109*, 315–335.
- (3) Ghasemi Afshar, P.; Honarvar, M.; Gharachorloo, M.; Eshratbadi, P.; Bazyar, B. Bleaching of Vegetable Oils Using Press Mud Obtained from Sugar Industry. *Pelagia Res. Libr. Eur. J. Exp. Biol.* **2014**, *4*, 677–684.
- (4) Silva, S. M.; Sampaio, K. A.; Ceriani, R.; Verh e, R.; Stevens, C.; De Greyt, W.; Meirelles, A. J. A. Effect of Type of Bleaching Earth on the Final Color of Refined Palm Oil. *Food Sci. Technol.* **2014**, *59*, 1258–1264.
- (5) Ismail, M. I.; Hamidon, M. H.; Zuhlilmie, M.; Sofi, M. Renewable Bleaching Alternatives (RBA) for Palm Oil Refining from Waste Materials Renewable Bleaching Alternatives (RBA) for Palm Oil Refining from Waste Materials. *J. Appl. Environ. Biol. Sci.* **2016**, *6*, 52–57.
- (6) Moreno, M.; Benavente, E.; Gonz alez, G.; Lavayen, V.; Torres, C. M. S. Functionalization of Bentonite by Intercalation of Surfactants. *Mol. Cryst. Liq. Cryst.* **2006**, *448*, 123–131.
- (7) Zhu, L.; Chen, B.; Shen, X. Sorption of Phenol, p-Nitrophenol, and Aniline to Dual-Cation Organobentonites from Water. *Environ. Sci. Technol.* **2000**, *34*, 468–475.
- (8) Chen, B.; Zhu, L.; Zhu, J.; Xing, B. Configurations of the Bentonite-Sorbed Myristylpyridinium Cation and Their Influences on the Uptake of Organic Compounds. *Environ. Sci. Technol.* **2005**, *39*, 6093–6100.
- (9) Anthony, S. Proteolytic Enzyme Cleaner. US Patent US6833408B22018.
- (10) Heilig, M. L. United States Patent Office. *ACM SIGGRAPH Comput. Graph.* **1994**, *28*, 131–134.
- (11) Karaca, S.; Gurses, A.; Ejder Korucu, M. Investigation of the Orientation of CTA + Ions in the Interlayer of CTAB Pillared Montmorillonite. *J. Chem.* **2013**, *2013*, DOI: 10.1155/2013/274838.
- (12) Acikyildiz, M.; Gurses, A.; Yolcu, H. H. Synthesis of Super Hydrophobic Clay by Solution Intercalation Method from Aqueous Dispersions. *Acta Phys. Pol., A* **2015**, *127*, 1156–1160.
- (13) Gunawan, N. S.; Indraswati, N.; Ju, Y. H.; Soetaredjo, F. E.; Ayucitra, A.; Ismadji, S. Bentonites Modified with Anionic and Cationic Surfactants for Bleaching of Crude Palm Oil. *Appl. Clay Sci.* **2010**, *47*, 462–464.
- (14) P erez-Santano, A.; Trujillano, R.; Belver, C.; Gil, A.; Vicente, M. A. Effect of the Intercalation Conditions of a Montmorillonite with Octadecylamine. *J. Colloid Interface Sci.* **2005**, *284*, 239–244.
- (15) Gu egan, R. Intercalation of a Nonionic Surfactant (C10E3) Bilayer into a Na-Montmorillonite Clay. *Langmuir* **2010**, *26*, 19175–19180.
- (16) Kurniawan, A.; Sutiono, H.; Ju, Y. H.; Soetaredjo, F. E.; Ayucitra, A.; Yudha, A.; Ismadji, S. Utilization of Rarasaponin Natural Surfactant for Organo-Bentonite Preparation: Application for Methylene Blue Removal from Aqueous Effluent. *Microporous Mesoporous Mater.* **2011**, *142*, 184–193.
- (17) Huang, Q.; Wang, W.; Yue, Y.; Hua, W.; Gao, Z. Delamination and Intercalation of Layered Aluminophosphate with [Al<sub>3</sub>P<sub>4</sub>O<sub>16</sub>]<sup>3-</sup> Stoichiometry in Water/Alcohol/Amine Solutions. *J. Colloid Interface Sci.* **2003**, *257*, 268–275.
- (18) Ismadji, S.; Soetaredjo, F. E.; Ayucitra, A. *Clay Materials for Environmental Remediation*; Springer International Publishing: Berlin, Germany, 2015.
- (19) Rosen, M. J. Relationship of Structure to Properties in Surfactants. III. Adsorption at the Solid-Liquid Interface from Aqueous Solution. *J. Am. Oil Chem. Soc.* **1975**, *52*, 431–435.
- (20) Motawie, A. M.; Madany, M. M.; El-Dakrory, A. Z.; Osman, H. M.; Ismail, E. A.; Badr, M. M.; El-Komy, D. A.; Abulyazied, D. E. Physico-Chemical Characteristics of Nano-Organo Bentonite Prepared Using Different Organo-Modifiers. *Egypt. J. Pet.* **2014**, *23*, 331–338.
- (21) Monteiro, M. K. S.; de Oliveira, V. R. L.; dos Santos, F. K. G.; de Barros Neto, E. L.; de Lima Leite, R. H.; Aroucha, E. M. M.; de Oliveira Silva, K. N. Influence of the Ionic and Nonionic Surfactants Mixture in the Structure and Properties of the Modified Bentonite Clay. *J. Mol. Liq.* **2018**, *272*, 990–998.
- (22) Gurses, A.; Gunes, K.; Mindivan, F.; Korucu, M. E.; Acikyildiz, M.; Dotar, C. The Investigation of Electrokinetic Behaviour of Micro-Particles Produced by CTA + Ions and Na-Montmorillonite. *Appl. Surf. Sci.* **2014**, *318*, 79–84.
- (23) Gurses, A.; Karaca, S.; Acikyildiz, M.; Ejder Korucu, M. Thermodynamics and Mechanism of Cetyltrimethylammonium Adsorption onto Clayey Soil from Aqueous Solutions. *Chem. Eng. J.* **2009**, *147*, 194–201.
- (24) Fabryanty, R.; Valencia, C.; Soetaredjo, F. E.; Putro, J. N.; Santoso, S. P.; Kurniawan, A.; Ju, Y. H.; Ismadji, S. Removal of Crystal Violet Dye by Adsorption Using Bentonite – Alginate Composite. *J. Environ. Chem. Eng.* **2017**, *5*, S677–S687.
- (25) Fiedor, J.; Burda, K. Potential Role of Carotenoids as Antioxidants in Human Health and Disease. *Nutrients* **2014**, *6*, 466–488.
- (26) Martin, H.-D.; J ager, C.; Ruck, C.; Schmidt, M.; Walsh, R.; Paust, J. Anti- and Prooxidant Properties of Carotenoids. *J. f ur Prakt. Chemie* **1999**, *341*, 302–308.
- (27) Moraes, D. S.; Miranda, L. C. R.; Ang elica, R. S.; Rocha Filho, G. N.; Zamian, J. R. Functionalization of Bentonite and Vermiculite after the Creation of Structural Defects through an Acid Leaching Process. *J. Braz. Chem. Soc.* **2018**, *29*, 320–327.
- (28) dos Santos, A.; Viante, M. F.; Pochapski, D. J.; Downs, A. J.; Almeida, C. A. P. Enhanced Removal of p-Nitrophenol from Aqueous Media by Montmorillonite Clay Modified with a Cationic Surfactant. *J. Hazard. Mater.* **2018**, *355*, 136–144.
- (29) Wu, Z.; Shang, T.; Deng, Y.; Tao, Y.; Yang, Q. H. The Assembly of MXenes from 2D to 3D. *Adv. Sci.* **2020**, *7*, No. 1903077.
- (30) Li, J.; Zhu, L.; Cai, W. Characteristics of Organobentonite Prepared by Microwave as a Sorbent to Organic Contaminants in Water. *Colloids Surf., A* **2006**, *281*, 177–183.
- (31) Widdyaningsih, L.; Setiawan, A.; Santoso, S. P.; Soetaredjo, F. E.; Ismadji, S.; Hartono, S. B.; Ju, Y. H.; Tran-Nguyen, P. L.; Yuliana, M. Feasibility Study of Nanocrystalline Cellulose as Adsorbent of Steryl Glucosides from Palm-Based Biodiesel. *Renewable Energy* **2020**, *154*, 99–106.
- (32) Chowdhury, S.; Mishra, R.; Saha, P.; Kushwaha, P. Adsorption Thermodynamics, Kinetics and Isothermic Heat of Adsorption of Malachite Green onto Chemically Modified Rice Husk. *Desalination* **2011**, *265*, 159–168.
- (33) Liu, Y.; Liu, Y. J. Biosorption Isotherms, Kinetics and Thermodynamics. *Sep. Purif. Technol.* **2008**, *61*, 229–242.
- (34) Speek, A. J.; Temalilwa, C. R.; Schrijver, J. Determination of  $\beta$ -Carotene Content and Vitamin A Activity of Vegetables by High-Performance Liquid Chromatography and Spectrophotometry. *Food Chem.* **1986**, *19*, 65–74.
- (35) Soufi, M. D.; Ghobadian, B.; Najafi, G.; Mohammad Mousavi, S.; Aubin, J. Optimization of Methyl Ester Production from Waste Cooking Oil in a Batch Tri-Orifice Oscillatory Baffled Reactor. *Fuel Process. Technol.* **2017**, *167*, 641–647.
- (36) Santosa, F. H.; Laysandra, L.; Soetaredjo, F. E.; Santoso, S. P.; Ismadji, S.; Yuliana, M. A Facile Noncatalytic Methyl Ester Production from Waste Chicken Tallow Using Single Step Subcritical Methanol: Optimization Study. *Int. J. Energy Res.* **2019**, *43*, 8852–8863.